PAPER

Characterization of InGaN quantum dots grown by metalorganic chemical vapor deposition

To cite this article: Caroline E Reilly et al 2019 Semicond. Sci. Technol. 34 125002

View the article online for updates and enhancements.

Recent citations

 Quantitative investigation of indium distribution in InN wetting layers and dots grown by metalorganic chemical vapor deposition Bastien Bonef et al



IOP ebooks™

Bringing together innovative digital publishing with leading authors from the global scientific community.

Start exploring the collection-download the first chapter of every title for free.

Semicond. Sci. Technol. 34 (2019) 125002 (7pp)

https://doi.org/10.1088/1361-6641/ab4b93

Characterization of InGaN quantum dots grown by metalorganic chemical vapor deposition

Caroline E Reilly¹, Bastien Bonef¹, Shuji Nakamura^{1,2}, James S Speck¹, Steven P DenBaars^{1,2} and Stacia Keller²

E-mail: cereilly@ucsb.edu

Received 27 August 2019, revised 19 September 2019 Accepted for publication 7 October 2019 Published 25 October 2019



Abstract

InGaN quantum dots were grown by metalorganic chemical vapor deposition and shown to exhibit a bimodal size distribution. Atom probe tomography was used to characterize the dots in conjunction with atomic force microscopy, photoluminescence, and x-ray diffraction. Small dots with low indium contents were found to coexist with larger, very high indium composition dots. Significant compositional fluctuations were observed in the small dot population. The dots showed abrupt interfaces with the surrounding GaN, verifying the ability to cap the dots without causing intermixing for even extremely high indium content dots.

Keywords: nitrides, atom probe tomography, metalorganic chemical vapor deposition, quantum dots

(Some figures may appear in colour only in the online journal)

1. Introduction

Applications such as highly efficient solid-state lighting and displays call for light-emitting diodes (LEDs) and laser diodes (LDs) that span the entire visible spectrum [1]. The nitrides semiconductor system has promised that the full visible spectrum can be provided by GaN-based devices. However, long wavelength emission into the green, amber, and red regions has proved difficult to achieve efficiently in GaN based devices. One of the reasons for this is the quantum confined Stark effect within c-plane oriented InGaN quantum wells (QWs), which is a polarization effect that decreases the overlap between the electron and hole wavefunctions. With higher indium concentration InGaN alloys, the higher strain to GaN causes stronger piezoelectric polarization effects, leading to larger electron and hole wavefunction separation and reduced efficiency in the active region. Proposed solutions include using non- and semi-polar planes [2-4], V-pit engineering [5, 6], and the replacement of QW active regions with quantum dot (QD) active regions [7-9]. All of these solutions can be attributed, in part, to polarization reduction in the active region of the device.

In the case of LDs, there are additional benefits in using QDs due to the three-dimensional confinement. When comparing the QD system to QWs, the QD system provides higher gain, lower threshold current, and less temperature dependence on the threshold current [10, 11]. QDs and dashes have proved useful for laser applications in other III–V systems, such as arsenides and phosphides [12–15]. QD active regions interact less with threading dislocations due to lateral carrier confinement [16], making them optimal for cases where the material quality is lower, such as epitaxial growth on mismatched substrates for photonic integrated circuits [17]. There is also evidence in the arsenide system for high reliability of QD based lasers [18, 19]. In the nitrides, InGaN QD lasers have been demonstrated by both molecular beam epitaxy and metalorganic chemical vapor deposition (MOCVD) growth [20–22].

Most InGaN QD work by MOCVD has focused on relatively low indium composition InGaN, with indium contents well under 50%. To make use of smaller sized, high density

1

 ¹ Materials Department, University of California, Santa Barbara, CA 93106, United States of America
² Electrical and Computer Engineering Department, University of California, Santa Barbara, CA 93106, United States of America

QDs, higher indium compositions need to be achieved due to the larger blue shift with increasing quantum confinement. Achieving higher indium content InGaN by MOCVD is challenging due to the differences in lattice constants and growth temperatures between InN and GaN. The 10% lattice mismatch between InN and GaN leads to relaxation of InN on GaN through the formation of misfit dislocations at the InN/GaN interface [23, 24]. While high quality MOCVD GaN is typically grown near 1100 °C, InN is typically grown at temperatures around 600 °C to prevent sublimation. For nitride LEDs and LDs, the composition of the InGaN OW active region is often controlled by varying the temperature, with lower temperatures corresponding to more indium. However, to achieve sufficiently high indium content with this method, temperatures would have to be in the range of those for InN growth. Lower growth temperatures can be problematic due to lower ammonia cracking efficiency, lower adatom surface mobility, and increased incorporation of carbon and oxygen impurities [25].

Despite the apparent incompatibility of InN and GaN, MOCVD studies have shown the growth of InN QDs on GaN with photoluminescence in the infrared [26–28]. Approaching high In composition InGaN growth from the low temperature growth conditions of InN has the advantage that In desorption, which is observed during InGaN growth at higher temperatures, is suppressed. However, when introducing gallium into InN to form InGaN QDs, another issue that has been reported is the realization of a bimodal distribution of InGaN into regions of lower and higher indium compositions, as discussed in the references [29-32]. In those systems, the lower indium composition dots are small in comparison to the higher indium composition dots. Directly characterizing the compositions of these separated regions has previously proved challenging, particularly due to redistribution of QDs upon capping [33]. Recent results have shown the ability to cap InN QDs grown on GaN, which allows for further characterization of buried structures through techniques such as atom probe tomography (APT) [27, 34].

Laser assisted APT has now extensively been applied for 3 dimensional nanometer scale characterizations of III-nitride semiconductors and devices [35, 36]. This technique can simultaneously provide geometrical and compositional information of nano-size features such as quantum wells [37, 38], QDs [39, 40], or even defects [41, 42]. Here, APT is particularly interesting to study compositional fluctuations of indium and gallium in the dots, as well as their shape and interface sharpness. These can be highly dependent on the MOCVD growth conditions of the samples. In this work, we have explored the growth of InGaN dots by MOCVD at a growth temperature of 565 °C and compositions of 50% indium and higher. Characterization has been performed via APT as well as atomic force microscopy (AFM), room temperature photoluminescence (PL), and x-ray diffraction (XRD).

2. Experiment

All growth experiments were conducted using an atmospheric MOCVD reactor with ammonia, triethylgallium (TEGa), trimethylgallium (TMGa), and triethylindium (TEIn) as precursors.

The dots were deposited on GaN-on-sapphire layers grown at high temperature with ammonia and TMGa *in situ* prior to InGaN dot deposition. The GaN layer underneath the dots was n-type doped with Si to grow the dots as if in an active region for a device structure. The binary InN and GaN growth rates were separately calibrated by growing thick layers on silicon and measuring the thickness with ellipsometry [23].

InGaN dots were grown at 565 °C, varying growth time and composition. The samples belonging to the growth time series were deposited with TEIn and TEGa flows corresponding to binary growth rates of 0.15 Å s⁻¹ for InN and $0.10 \,\text{Å s}^{-1}$ for GaN, resulting in an InN to GaN growth rate ratio, r(InN):r(GaN), of 3:2. Deposition times were 25, 50, 150, and 500 s. The corresponding nominal planar InGaN layer thicknesses were 0.5 nm, 1 nm, 3 nm, and 10 nm, respectively. A compositional series was grown with a constant growth time of 150 s and r(InN):r(GaN) ratios of 3:1, 3:2, and 1:1. In this series, the TEIn flow was kept constant and corresponded to a nominal InN growth rate of 0.15 Å s^{-1} . The TEGa flow was varied, with the total nominal InGaN growth rate of the dots being $0.20 \,\mathrm{\mathring{A}}\,\mathrm{s}^{-1}$ (3:1), $0.25 \,\mathrm{\mathring{A}}\,\mathrm{s}^{-1}$ (3:2), and 0.30 Å s^{-1} (1:1). In addition one sample was grown with an InGaN growth time of 50 s and a r(InN):r(GaN) ratio of 3:2, which was capped with 5.8 nm of n-type Si-doped GaN grown with TEGa directly after the InGaN at the same temperature as the dots. To facilitate the preparation of APT tips, a 140 nm thick polycrystalline GaN cap was deposited via MOCVD on the capped sample with TEGa and TMGa at 565 °C as a regrowth after initial analysis.

AFM was conducted on all samples using an Asylum MFP-3D with scan sizes of $(1.5~\mu\text{m})^2$. Room temperature infrared PL measurements were taken using a liquid nitrogen cooled InGaAs detector and excitation with a 780 nm laser incident on the sample through a microscope objective (the objective lens was also used to collect to the luminescence). The detector allowed data collection from 800 to 1550 nm. Room temperature visible PL was collected using a HeCd laser emitting at 325 nm. XRD ω -2 θ scans were taken for the compositional series around the (0002) GaN peak with a Panalytical MRD PRO. The indium composition of the grown material was extracted from the XRD scans using the Panalytical Epitaxy software.

A FEI Helios 600 dual beam FIB instrument was used for the preparation of the needle shaped samples for the APT analysis [43]. The APT analyzes were performed with a Cameca 3000X HR Local Electrode Atom Probe operated in laser-pulse mode (13 ps pulse, 532 nm green laser, $10\,\mu\mathrm{m}$ laser spot size) with a sample based temperature of 30 K. The laser pulse energy and the detection rate for the experiments were respectively set to 0.5 nJ and 0.01 atoms per pulse. The 3D reconstruction were carried out using a geometrical based algorithm implemented in the commercial software IVASTM [44].

3. Results and discussion

Figure 1 shows the evolution of the InGaN dots with increasing growth time at a constant r(InN):r(GaN) ratio of

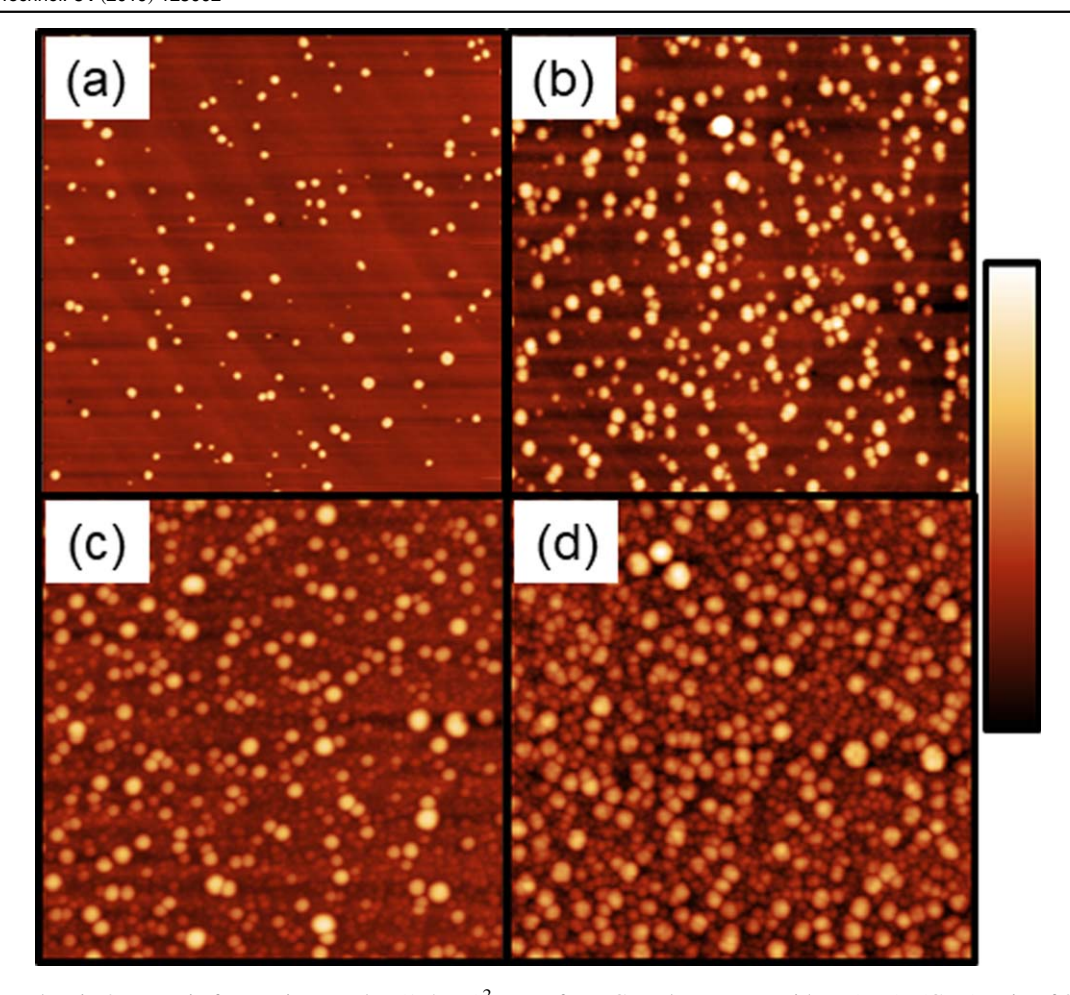


Figure 1. InGaN dots in 2D atomic force micrographs; $(1.5 \mu m)^2$ scans for InGaN dots grown with a r(InN):r(GaN) ratio of 3:2 and growth times of (a) 25 s, (b) 50 s, (c) 150 s, and (d) 500 s. Scale bar from 0 to 17 nm for (a),(b) and 0 to 50 nm for (c), (d).

3:2. In this series, initially only one dot population can be seen (figure 1(a)) before a few smaller dots appear by a growth time of 50 s (figure 1(b)), with a bimodal distribution visible at longer growth times (figures 1(c), (d)). The larger dots about doubled in density between 25 and 50 s, reaching a density of around $1.3 \times 10^{10} \, \text{cm}^{-2}$ at a growth time of 50 s. No significant change in density was observed when the deposition time was further increased to 500 s. The large dots showed little change in height between 25 s (8 nm) and 50 s (10 nm) but grew upwards between 50 and 150 s to a height of about 21 nm, after which the height remained unchanged. The width of the dots increased from about 40 to 62 nm when the growth time was increased from 25 to 50 s but exhibited an only modest increase to about 71 and 77 nm when the growth time was further increased to 150 s and 500 s, respectively. The smaller dots did not appear on the scale of the AFM image for the sample with a growth time of 25 s but were clearly visible at a growth time of 150 s. Their diameters increased slightly from about 36 to 43 nm between growth times of 150 and 500 s. Simultaneously, their height increased from 4 to 8 nm. Note that the circular shape of the dots in the AFM images may be an AFM tip effect, and that the apparent dot sizes may be considered as upper limits.

Figure 2 shows the room temperature IR PL spectra taken from the samples belonging to the time series, with a detector limited upper wavelength of 1550 nm. The fringes in the PL spectrum were Fabry-Pérot fringes caused by the interference from the GaN/sapphire interface. All samples showed infrared emission from the dots. Peak wavelengths for the two thicker samples were the same at around 1280 nm, suggesting that there was no additional quantum confinement or compositional change for the 150 s compared to the 500 s sample. As the expected luminescence wavelength for pure bulk InN was 1770 nm, outside of the range of the detector, the emission at 1280 nm was likely associated with some gallium incorporation in the dots. The blue shift of about 100 nm for the 50 s sample was attributed to quantum confinement effects due to the lower height of the large dots as observed by AFM. The 25 s sample had low PL intensity, but the peak appeared to be blue shifted by another 100 nm from the 50 s sample consistent with an increased quantum confinement. In addition to the blue shift, the intensity decreased as the growth time decreased for all samples, as would be expected due to the smaller amount of light emitting material.

Figure 3 displays the AFM images of the samples from the compositional series in which the amount of Ga precursor

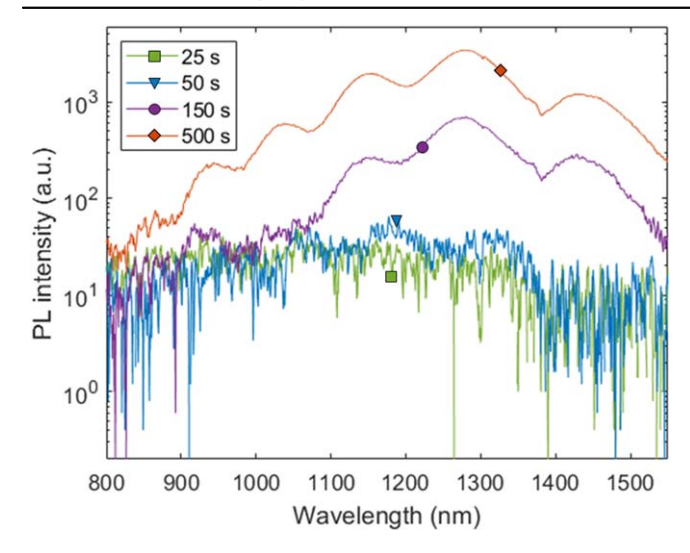


Figure 2. Infrared photoluminescence at 300 K with 780 nm laser excitation for InGaN dot samples with growth times from 25 to 500 s.

injected during dot growth was varied. All samples showed a bimodal distribution of larger and smaller dots via AFM. Particularly for the two samples grown with higher TEGa flows, the dots appeared to align along steps of the underlying GaN. With increasing TEGa flow for the dots, the large dots became smaller and their density decreased whereas the density of the small dots increased. This suggested that the larger dots may have had a higher indium content and the smaller dots a lower indium content.

Figure 4 shows the room temperature IR PL spectra for the compositional series samples. As more TEGa was added to the gas phase, the PL blue shifted and decreased in intensity, corresponding to the larger dots having decreased in size and density. The peak wavelength for the sample grown with the lowest TEGa flow was above 1550 nm and thus outside of the range of the detector, indicating the presence of dots with a very low amount of gallium. The PL peak for the mid-range composition sample centered around 1230 nm and the peak for the sample with the highest TEGa flow was about 1150 nm. As the growth time series showed a similar degree of blue shift and intensity with decreasing dot sizes, a significant degree of this shift and intensity drop in this series could have been associated with increased confinement effects in the high indium composition dots, which decreased in size and density with increasing TEGa flow as well.

For both the time and composition series, visible PL was also collected using a HeCd laser. Yellow luminescence from the underlying n-GaN:Si dominated the spectra. As the samples in both series were uncapped, the lack of luminescence was not unexpected due to InGaN surface band bending resulting in a lack of carriers. In comparison, the very high indium composition dots with a significantly smaller bandgap may exhibit an electron accumulation near the surface similar to that known for InN, enabling the observation of luminescence [28]. Additionally, if carriers were not well confined within the InGaN dots and were able to move, they would

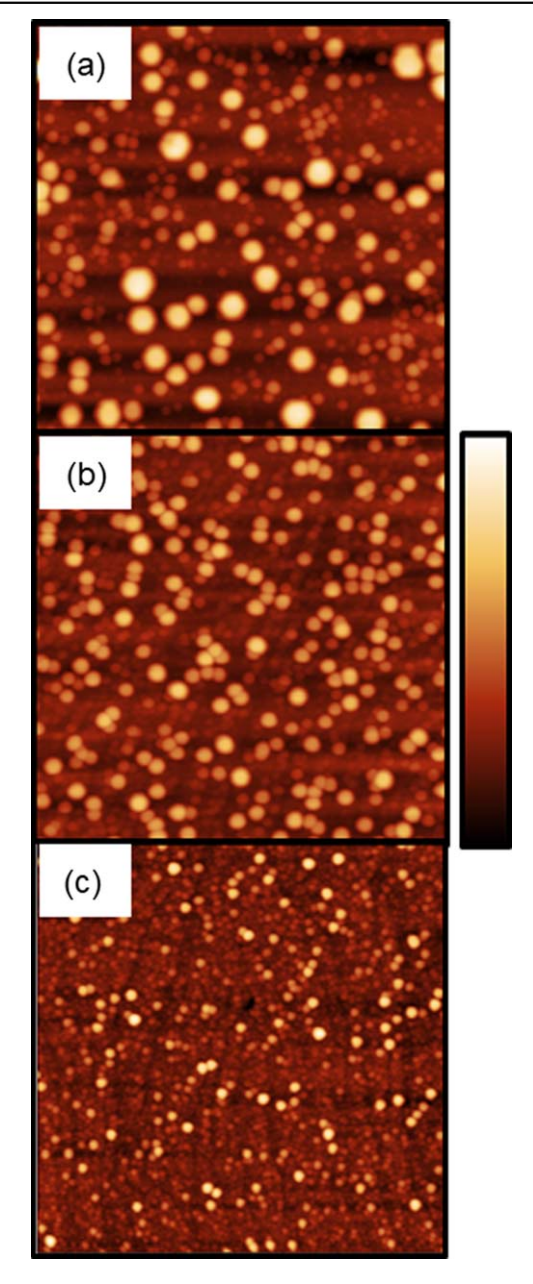


Figure 3. InGaN dots in 2D atomic force micrographs; $(1.5 \mu m)^2$ scans for InGaN dot samples grown with r(InN):r(GaN) ratios of (a) 3:1, (b) 3:2, and (c) 1:1. The deposition time was 150 s. Scale bar from 0 to 50 nm for (a/b) and 0 to 27 nm for (c).

have fallen into the potential wells of the dots with higher indium compositions.

XRD ω -2 θ scans measured on the composition series are shown in figure 5 to further analyze the dot composition. The tall sharp peak corresponded to the GaN (0002) peak in each sample. The existence of a peak around 15.7° near that expected for relaxed InN as well as the shoulder on the left side of the GaN peak, which increased in intensity with increasing TEGa precursor flow, further support the existence of a bimodal dot population. Due to the peaks being broad, it was difficult to assign accurate compositions. The sample with the lowest gallium content showed a defined XRD peak close to that of the relaxed InN (0002) peak, indicating very

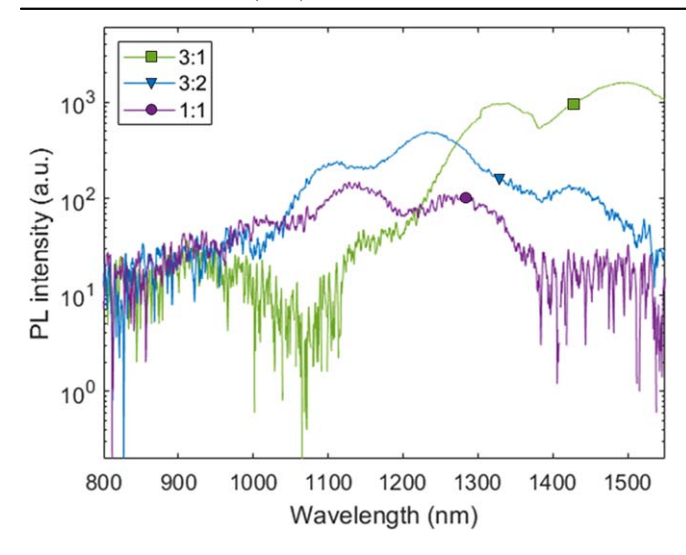


Figure 4. Infrared photoluminescence at 300 K with 780 nm laser excitation for InGaN dot samples grown with different r(InN):r(GaN) ratios.

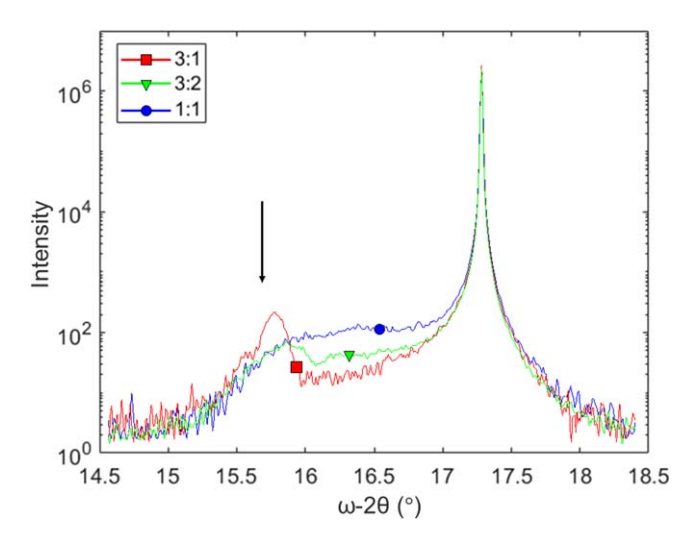


Figure 5. X-ray diffraction (XRD) ω -2 θ scans showing the (0002) peaks for GaN and InN for the InGaN dot samples grown with different r(InN):r(GaN) ratios. Arrow indicates relaxed InN (0002) peak position.

little gallium content, consistent with the PL being over 1550 nm in peak wavelength for the same sample. The XRD peak of the In rich dots decreased in intensity and shifted somewhat towards the GaN peak as gallium precursor injection was increased, consistent with the decreasing size and density of the larger, In rich dots observed in the AFM images. Simultaneously, the InGaN shoulder adjacent to the GaN peak increased in intensity, indicating the increased presence of material with lower indium compositions. As the AFM images taken from the composition series samples showed an increase in the small dot population with an increase in TEGa flow, the shoulder peak was attributed to the small dot population.

For the highest gallium precursor flow, the two peaks cannot be resolved, and the AFM images for the same sample showed the larger dots becoming smaller and sparser. The infrared PL remained for this sample, suggesting that the lack of resolution of the XRD peaks was due to the lower intensity of the peak near InN and not necessarily the dot populations merging. The broadness of the InGaN shoulder peak would be consistent with significant compositional fluctuations in the small InGaN dots, such that the small dot population did not have a well-defined composition.

Figure 6 shows the APT data of the capped InGaN sample with an InGaN growth time of 50 s, where the analysis of the uncapped sample showed primarily InN rich dots. The APT data allowed for the site-specific observation of the In distributions within and outside the dots, which cannot be obtained using XRD. Additionally, the shape and size of the dots could be obtained. Figure 6(a) shows a 3D side view of a large dot. The population of large dots in this sample was significant enough to capture a dot in an APT sample without prior site-specific preparation procedure. Only four tips were evaporated here to have one containing a dot. A top view of the dot, evidenced by an In iso-concentration surface [45], is shown in figure 6(b). The dot appeared to have a truncated hexagonal pyramid shape with a flat top interface and well-defined sharp side facets. At the bottom interface, the dot appeared to be around 20 nm wide and its height was about 15 nm. Figure 6(c) shows a 2D concentration map of In in the dot, extracted from the volume indicated in figure 6(b). The In projection was projected along the Y direction in a $26 \times 5 \times 20 \text{ nm}^3$ sampling volume. Voxel size and delocalization parameters to calculate local In compositions were respectively 0.5 nm and 2 nm in all directions [46]. The truncated hexagonal pyramid shape of the dot was clearly obtained from figure 6(c). Bottom, top and side interfaces appeared to be similar according to the In distribution and no significant In incorporation was observed in the GaN cap layer. A high In fraction above 0.8 was observed in all the dot. The highest In fraction of 1 was measured in the bottom part of the dot with a progressive incorporation of Ga observed moving closer to the top interface. A 1D concentration profile showing the In concentration in the dot along the [0001] growth direction is shown in figure 6(d). As already observed in figure 6(c), the dot was pure InN close to the bottom interface with a progressive incorporation of Ga which did not exceed a III site fraction of 0.2.

4. Conclusions

In conclusion, InGaN dots were grown by MOCVD. The bimodal population of dots showed room temperature infrared photoluminescence consistent with the presence of very high In composition dots, which was confirmed by APT analysis. The larger hexagonal dots that were nearly pure InN existed alongside smaller, flatter dots with lower indium composition. The high In composition dots showed abrupt interfaces with the surrounding GaN, providing evidence that there was minimal intermixing when the GaN cap was grown. The lack of intermixing when capping opens the potential to work with high indium content designs in future InGaN QD systems.

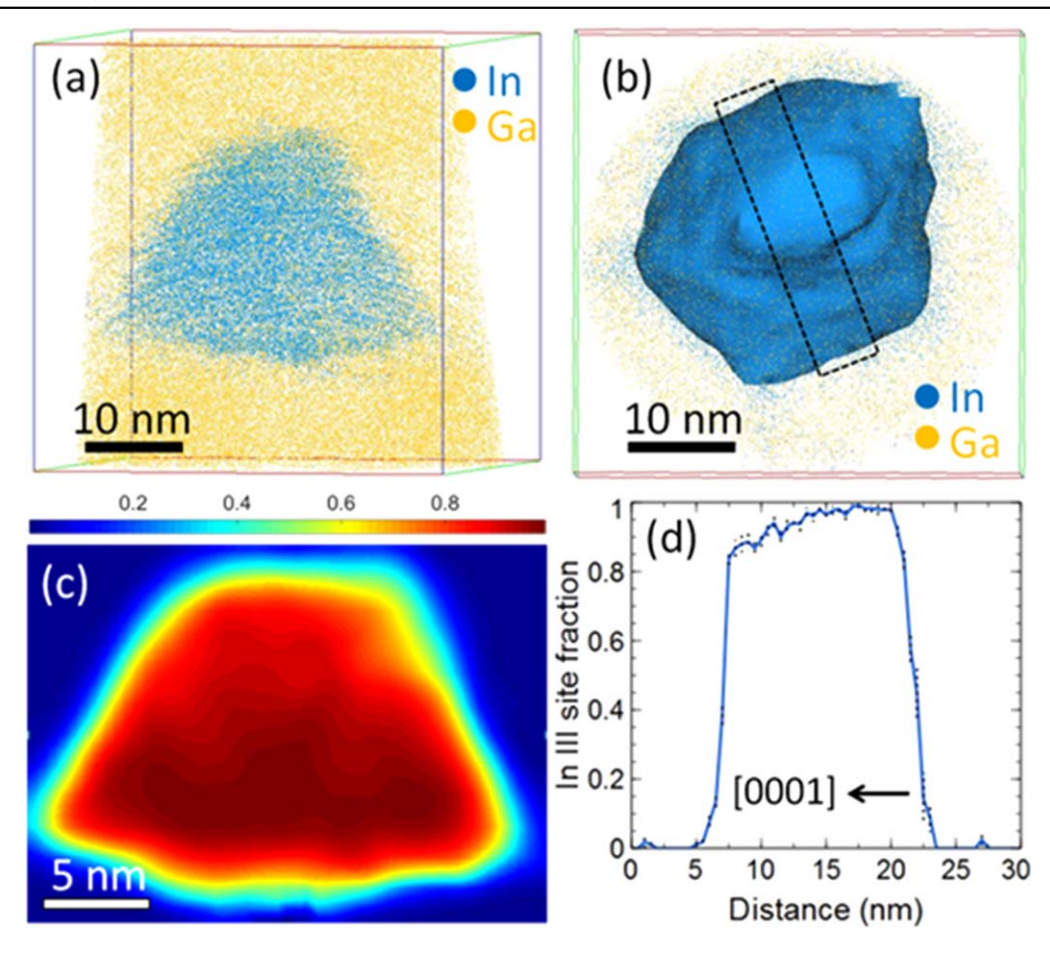


Figure 6. (a) APT 3D reconstruction of a single dot. (b) Top view of the dot evidenced by a 50% In iso-concentration surface. (c) 2D side view of the In distribution in the dot and extracted from the dashed region in (b). (d) 1D concentration profile of In in the dot along the [0001] growth direction.

Acknowledgments

This work was supported by the Solid State Lighting and Energy Electronics Center (SSLEEC) at the University of California, Santa Barbara. This work was supported by a grant from the Simons Foundation (601952, JS). This research was supported (BB and JSS) in part by the NSF RAISE-TAQS program number 1839077 through a subcontract from the University of Minnesota. The research reported here made use of shared facilities of the UCSB MRSEC (NSF DMR 1720256).

ORCID iDs

Caroline E Reilly https://orcid.org/0000-0002-9422-1159 Stacia Keller https://orcid.org/0000-0002-6529-3516

References

 Phillips J M et al 2007 Research challenges to ultra-efficient inorganic solid-state lighting Laser Photonics Rev. 1 307–33

- [2] Feezell D F, Schmidt M C, DenBaars S P and Nakamura S 2009 Development of nonpolar and semipolar InGaN/GaN visible light-emitting diodes MRS Bull. 34 318–23
- [3] Park S-H and Chuang S-L 1999 Crystal-orientation effects on the piezoelectric field and electronic properties of strained wurtzite semiconductors *Phys. Rev.* B 59 4725–37
- [4] Waltereit P, Brandt O, Trampert A, T Grahn H T, Menniger J, Ramsteiner M, Reiche M and Ploog K H 2000 Nitride semiconductors free of electrostatic fields for efficient white light-emitting diodes *Nature* 406 865–8
- [5] Hangleiter A, Hitzel F, Netzel C, Fuhrmann D, Rossow U, Ade G and Hinze P 2005 Suppression of nonradiative recombination by V-shaped pits in GaInN/GaN quantum wells produces a large increase in the light emission efficiency *Phys. Rev. Lett.* 95 127402
- [6] Jiang F et al 2019 Efficient InGaN-based yellow-light-emitting diodes Photonics Res. 7 144
- [7] Wierer J J, Tansu N, Fischer A J and Tsao J Y 2016 III-nitride quantum dots for ultra-efficient solid-state lighting *Laser Photonics Rev.* 10 612–22
- [8] Wu Y-R, Lin Y-Y, Huang H-H and Singh J 2009 Electronic and optical properties of InGaN quantum dot based light emitters for solid state lighting J. Appl. Phys. 105 013117
- [9] Schulz S and O'Reilly E P 2010 Theory of reduced built-in polarization field in nitride-based quantum dots *Phys. Rev.* B 82 033411
- [10] Asada M, Miyamoto Y and Suematsu Y 1986 Gain and the threshold of three-dimensional quantum-box lasers *IEEE J. Quantum Electron.* QE-22 1915–21

- [11] Arakawa Y and Sakaki H 1982 Multidimensional quantum well laser and temperature dependence of its threshold current Appl. Phys. Lett. 40 939–41
- [12] Kirstaedter N et al 1994 Low threshold, large To injection laser emission from (InGa)As quantum dots Electron. Lett 30 1416–7
- [13] Wang R H, Stintz A, Varangis P M, Newell T C, Li H, Malloy K J and Lester L F 2001 Room-temperature operation of InAs quantum-dash lasers on InP *IEEE Photonics Technol. Lett.* 13 767–9
- [14] Kaiander I N, Sellin R L, Kettler T, Ledentsov N N, Bimberg D, Zakharov N D and Werner P 2004 1.24 um InGaAs/GaAs quantum dot laser grown by metalorganic chemical vapor deposition using tertiarybutylarsine Appl. Phys. Lett. 84 2992–4
- [15] Leonard D, Krishnamurthy M, Reaves C M, Denbaars S P and Petroff P M 1993 Direct formation of quantum-sized dots from uniform coherent islands of InGaAs on GaAs surfaces Appl. Phys. Lett. 63 3203–5
- [16] Gérard J M, Cabrol O and Sermage B 1996 InAs quantum boxes: Highly efficient radiative traps for light emitting devices on Si Appl. Phys. Lett. 68 3123–5
- [17] Mi Z, Yang J, Bhattacharya P, Qin G and Ma Z 2009 Highperformance quantum dot lasers and integrated optoelectronics on Si *Proc. IEEE* 97 1239–49
- [18] Liu A Y, Herrick R W, Ueda O, Petroff P M, Gossard A C and Bowers J E 2015 Reliability of InAs/GaAs quantum dot lasers epitaxially grown on silicon *IEEE J. Sel. Top. Quantum Electron.* 21 690–7
- [19] Sellin R L, Ribbat C, Bimberg D, Rinner F, Konstanzer H, Kelemen M T and Mikulla M 2002 High-reliability MOCVD-grown quantum dot laser *Electron. Lett* 38 883–4
- [20] Zhang M, Banerjee A, Lee C-S, Hinckley J M and Bhattacharya P 2011 A InGaN/GaN quantum dot green (524 nm) laser Appl. Phys. Lett. 98 221104
- [21] Frost T, Hazari A, Aiello A, Zunaid Baten M, Yan L, Mirecki-Millunchick J and Bhattacharya P 2016 High performance red-emitting multiple layer InGaN/GaN quantum dot lasers *Japan. J. Appl. Phys.* 55 032101
- [22] Weng G, Mei Y, Liu J, Hofmann W, Ying L, Zhang J, Bu Y, Li Z, Yang H and Zhang B 2016 Low threshold continuouswave lasing of yellow-green InGaN-QD vertical-cavity surface-emitting lasers Opt. Express 24 15546–53
- [23] Lund C, Catalano M, Wang L, Wurm C, Mates T, Kim M, Nakamura S, DenBaars S P, Mishra U K and Keller S 2018 Metal-organic chemical vapor deposition of N-polar InN quantum dots and thin films on vicinal GaN J. Appl. Phys. 123 055702
- [24] Lozano J G, Sánchez A M, García R, Ruffenach S, Briot O and González D 2007 Strain relief analysis of InN quantum dots grown on GaN *Nanoscale Res. Lett.* 2 442–6
- [25] Lund C, Nakamura S, DenBaars S P, Mishra U K and Keller S 2017 Growth of high purity N-polar (In, Ga)N films J. Cryst. Growth 464 127–31
- [26] Ruffenach S, Maleyre B, Briot O and Gil B 2005 Growth of InN quantum dots by MOVPE *Phys. Status Solidi* c 2 826–32
- [27] Reilly C E, Lund C, Nakamura S, Mishra U K, Denbaars S P and Keller S 2019 Infrared luminescence from N-polar InN quantum dots and thin films grown by metal organic chemical vapor deposition Appl. Phys. Lett. 114 241103
- [28] Ku C S, Chou W C and Lee M C 2007 Optical investigations of InN nanodots capped by GaN at different temperatures Appl. Phys. Lett. 90 132116
- [29] Ho I-H and Stringfellow G B 1996 Solid phase immiscibility in GaInN Appl. Phys. Lett. 69 2701–3

- [30] El-Masry N A, Piner E L, Liu S X and Bedair S M 1998 Phase separation in InGaN grown by metalorganic chemical vapor deposition Appl. Phys. Lett. 72 40–2
- [31] Tessarek C, Figge S, Aschenbrenner T, Bley S, Rosenauer A, Seyfried M, Kalden J, Sebald K, Gutowski J and Hommel D 2011 Strong phase separation of strained InxGa1-xN layers due to spinodal and binodal decomposition: Formation of stable quantum dots *Phys. Rev.* B 83 115316
- [32] Figge S, Tessarek C, Aschenbrenner T and Hommel D 2011 Ingan quantum dot growth in the limits of Stranski– Krastanov and spinodal decomposition *Phys. Status Solidi* B 248 1765–76
- [33] Wang Q, Wang T, Bai J, Cullis A G, Parbrook P J and Ranalli F 2008 Influence of annealing temperature on optical properties of InGaN quantum dot based light emitting diodes Appl. Phys. Lett. 93 081915
- [34] Reilly C E, Nakamura S, DenBaars S P and Keller S 2019 MOCVD growth and characterization of InN quantum dots *Phys. Status Solidi* B (https://doi.org/10.1002/ pssb.201900508)
- [35] Rigutti L, Bonef B, Speck J, Tang F and Oliver R A 2018 Atom probe tomography of nitride semiconductors *Scripta Materialia* 148 75–81
- [36] Bonef B, Catalano M, Lund C, Denbaars S P, Nakamura S, Mishra U K, Kim M J and Keller S 2017 Indium segregation in N-polar InGaN quantum wells evidenced by energy dispersive x-ray spectroscopy and atom probe tomography Appl. Phys. Lett. 110 143101
- [37] Khoury M, Li H, Bonef B, Kuritzky L Y, Mughal A J, Nakamura S, Speck J S and DenBaars S P 2018 Semipolar (20-21) GaN templates on sapphire: 432 nm InGaN lightemitting diodes and light extraction simulations Appl. Phys. Express 11 036501
- [38] Li H *et al* 2017 Efficient semipolar (11–22) 550 nm yellow/green InGaN light-emitting diodes on low defect density (11–22) GaN/sapphire templates *ACS Appl. Mater. Interfaces* **9** 36417–22
- [39] Mancini L et al 2014 Three-dimensional nanoscale study of Al segregation and quantum dot formation in GaAs/AlGaAs core-shell nanowires Appl. Phys. Lett. 105 243106
- [40] Hernández-Saz J, Herrera M, Molina S I, Stanley C R and Duguay S 2016 Atom probe tomography analysis of InAlGaAs capped InAs/GaAs stacked quantum dots with variable barrier layer thickness Acta Mater. 103 651–7
- [41] Bonef B, Shah R D and Mukherjee K 2019 Fast Diffusion and segregation along threading dislocations in semiconductor heterostructures *Nano Lett.* 19 1428–36
- [42] Usami S, Mayama N, Toda K, Tanaka A, Deki M, Nitta S, Honda Y and Amano H 2019 Direct evidence of Mg diffusion through threading mixed dislocations in GaN p-n diodes and its effect on reverse leakage current Appl. Phys. Lett. 114 232105
- [43] Thompson K, Lawrence D, Larson D J, Olson J D, Kelly T F and Gorman B 2007 *In situ* site-specific specimen preparation for atom probe tomography *Ultramicroscopy* 107 131–9
- [44] Vurpillot F, Gault B, Geiser B P and Larson D J 2013 Reconstructing atom probe data: a review *Ultramicroscopy* 132 19–30
- [45] Hellman O C, Vandenbroucke J A, Rüsing J, Isheim D and Seidman D N 2000 Analysis of three-dimensional atomprobe data by the proximity histogram *Microsc. Microanal*. 6 437–44
- [46] Torres K L, Daniil M, Willard M A and Thompson G B 2011 The influence of voxel size on atom probe tomography data *Ultramicroscopy* 111 464–8